AGU PUBLICATIONS

JGR

Journal of Geophysical Research: Atmospheres

RESEARCH ARTICLE
10.1002/2016JD024959

Key Points:
- Impact of model horizontal resolution of BCC_CSM model
- Precipitation seasonal variation over eastern China

Correspondence to:
A. Huang,
anhuang@nju.edu.cn

Citation:
Wang, Q., A. Huang, Y. Zhao, Y. Zhou, B. Yang, L. Zhang, H. Wu, Y. Jiang, and M. Kan (2016), Evaluation of the precipitation seasonal variation over eastern China simulated by BCC_CSM model with two horizontal resolutions, *J. Geophys. Res. Atmos.*, *121*, 8374–8389, doi:10.1002/2016JD024959.

Received 16 FEB 2016
Accepted 9 JUL 2016
Accepted article online 12 JUL 2016
Published online 28 JUL 2016

Evaluation of the precipitation seasonal variation over eastern China simulated by BCC_CSM model with two horizontal resolutions

Qian Wang[1], Anning Huang[1], Yong Zhao[2], Yang Zhou[1], Ben Yang[1], Lujun Zhang[1], Haomin Wu[3], Yanmin Jiang[3], and Mengyun Kan[1]

[1]CMA-NJU Joint Laboratory for Climate Prediction Studies, School of Atmospheric Sciences, Nanjing University, Nanjing, China, [2]School of Atmospheric Sciences, Chendu University of Information Technology, Chengdu, China, [3]Lishui Meteorological Bureau, Lishui, China

Abstract The performance of Beijing Climate Center climate system model (BCC_CSM) with two horizontal resolutions in simulating the precipitation seasonal variation over eastern China has been evaluated. The possible reasons related to the differences in the simulations of BCC_CSM1.1 m model with fine resolution and BCC_CSM1.1 model with coarse resolution also have been addressed and discussed. Results show that the improved simulation of the timing and amount of precipitation in dry seasons except for larger biases during rainy seasons can be noted in BCC_CSM1.1 m model relative to BCC_CSM1.1 model. The occurrence time of the precipitation annual peaks in BCC_CSM1.1 m model shows better agreements with the observation compared to BCC_CSM1.1 model. Mechanism analysis indicates that BCC_CSM1.1 produced earlier East Asian summer monsoon (EASM) onset and northward jump of western Pacific subtropical high (WPSH), leading to the earlier start of the rainy seasons and occurrence time of the precipitation annual peaks over eastern China comparing with the observation and BCC_CSM1.1 m simulation. The improved EASM onset and northward jump of WPSH in BCC_CSM1.1 m model resulted in better simulation of precipitation seasonal transition and occurrence time of the precipitation annual peaks. However, compared to BCC_CSM1.1 model, the much more underestimated summer precipitation over most eastern China in BCC_CSM1.1 m model is mainly due to the weakly simulated northeastward water vapor transport, which is resulted from the much stronger WPSH with farther northwest location and weaker land-sea thermal contrast.

1. Introduction

Due to the complex terrain (Figure 1), climates over China show large temporal and spatial variations. In addition to the topography, the East Asia monsoon which affects the eastern seashores more than inland areas in northwestern China is another factor that can lead to the great seasonal and regional differences in precipitation across China [*Ding and Chan*, 2005; *Liu et al*., 2005]. However, most current climate models still cannot simulate the changes in the climate characteristics especially precipitation over eastern China well [*Rajendran et al*., 2004; *Ding et al*., 2007; *Huang et al*., 2015].

Earlier studies have shown that high-resolution modeling can provide more details of fine-scale forcings (e.g., topography and land use), which are important for the application of climate information such as seasonal climate forecasts and long-term climate projections in the impact assessment [*Leung and Qian*, 2003; *Li et al*., 2015]. Horizontal resolution plays an important role in both climate system models (CSMs) and regional climate models (RCMs) [*Giorgi and Marinucci*, 1996; *Duffy et al*., 2003; *Gao et al*., 2006a, 2006b; *Sara et al*., 2010; *Gao et al*., 2011]. RCMs may run at high horizontal resolutions over limited areas, permitting them to capture fine-scale climate forcings [*Boville,* 1991; *Giorgi and Mearns*, 1991]; however, high dependence on the lateral boundary conditions limits their applications in long-term climate predictions. As grand geophysical laboratories, CSMs can objectively depict the interactions among atmosphere, cryosphere, biosphere, lithosphere, and hydrosphere [*Huang et al*., 2014]. They are powerful tools for both enhancing our understanding of the fundamental mechanisms of the climate system and scenario projections of the future climate change [*Zhou et al*., 2007; *Li et al*., 2015; *Ning and Bradley*, 2016]. With the development of computing resources and the growing needs of regional climate information, CSMs may apply relatively high spatial resolutions, which allow them to better resolve the surface characteristics

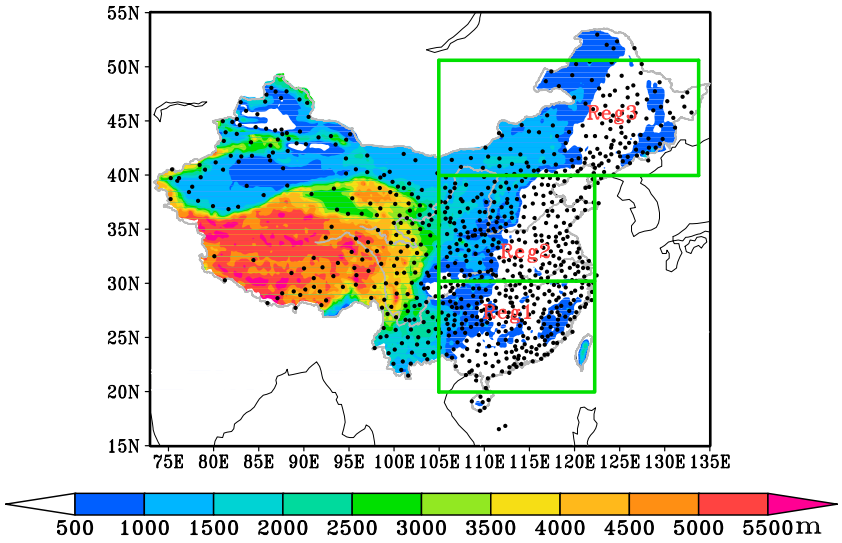

Figure 1. Locations of the observation stations (black dots) and the terrain height (shadings). The three subregions over eastern China are denoted by green rectangles. The Yangtze River and Yellow River are indicated by grey curves.

and represent the processes and interactions (e.g., fine-scale structure of synoptic and mesoscale systems or cloud complexes) [*Tibaldi et al.*, 1990; *Sperber et al.*, 1994; *Senior*, 1995; *Giorgi and Marinucci*, 1996; *Leung and Qian*, 2003; *Gao et al.*, 2006a; *Rauscher et al.*, 2010]. Horizontal resolution is one of major factors that affects the models' performance [*Mass et al.*, 2002; *Zhou and Li*, 2002; *Leung and Qian*, 2003; *Navarra et al.*, 2008; *Jung et al.*, 2012; *Hertwig et al.*, 2015; *Ramu et al.*, 2016]. Some studies have shown that increasing horizontal resolution can lead to a better representation of the general circulation of the atmosphere, which in turn would affect the simulation of large-scale flow features determining the climate characteristics in a given region [*Giorgi and Marinucci*, 1996; *Leung and Qian*, 2003; *Shiao and Juang*, 2006; *Tripathi and Dominguez*, 2013; *Jiang et al.*, 2015; *Li et al.*, 2015]. However, some studies also indicate that the performance of climate models with fine resolution is not improved over some regions relative to those with coarse resolution [*Boyle*, 1993; *Giorgi and Marinucci*, 1996; *Marshall et al.*, 1997; *Mass et al.*, 2002; *Duffy et al.*, 2003; *Wehner et al.*, 2010; *Kan et al.*, 2015].

In recent years the Beijing Climate Center (BCC) has developed the climate system model (CSM) with two versions: BCC_CSM1.1 with coarse resolution (T42 or approximately 280 km) and BCC_CSM1.1 m with moderate resolution (T106 or approximately 110 km) [*Huang et al.*, 2013; *Wu et al.*, 2008, 2010, 2014; *Yang et al.*, 2015]. Both versions of the BCC_CSM model have participated in the Coupled Model Intercomparison Project phase 5 (CMIP5) experiments of the Intergovernmental Panel on Climate Change Fifth Assessment Report [*Xin et al.*, 2012; *Wu et al.*, 2014]. Many previous studies have evaluated the performance of the two models in simulating surface air temperature [*Gao et al.*, 2012; *Xin et al.*, 2013a, 2013b; *Jiang et al.*, 2015] and precipitation globally and regionally [*Zhang et al.*, 2013; *Wu et al.*, 2014; *Kan et al.*, 2015], suggesting that the performance of both models is comparable to that of other CMIP5 models. Although BCC_CSM1.1 m model shows better ability in simulating the spatial distribution of precipitation over many regions of the globe such as those with complex terrains than BCC_CSM1.1 model, much larger precipitation biases over eastern China dominated by monsoonal climates can be noted in BCC_CSM1.1 m model [*Wu et al.*, 2014; *Kan et al.*, 2015]. In addition, how the performance of both models in simulating the precipitation seasonal variation over eastern China [*Ding and Chan*, 2005; *Liu et al.*, 2005; *Huang et al.*, 2007; *Zhu et al.*, 2011] is still unclear so far. It is necessary to evaluate the performance of both versions of BCC_CSM model in simulating the precipitation seasonal variation over eastern China.

Previous studies mostly concentrated on the model's performance in simulating the seasonal mean precipitation over eastern China; few studies have evaluated the performance of BCC_CSM1.1 and BCC_CSM1.1 m models in simulating the precipitation seasonal variation over eastern China. Evaluating the timing of precipitation simulated by BCC_CSM model with different horizontal resolutions and revealing the differences in

the simulations of different versions of BCC_CSM model and possible associated causes are very important for further improving the skills of seasonal forecasts over eastern China. In this study, we focus on evaluating the seasonal variation of precipitation over eastern China simulated by BCC_CSM model with two horizontal resolutions and revealing whether the model performance is improved or not by only increasing model horizontal resolution. Moreover, the possible causes related to the improvements or deterioration of BCC_CSM1.1 m simulation relative to BCC_CSM1.1 simulation are also discussed. Results obtained in this study may provide some necessary information to further develop the BCC_CSM model with fine horizontal resolution.

Section 2 gives the model, data, and methodology. Section 3 exhibits the performance of both versions of BCC_CSM model in simulating the precipitation seasonal variation over eastern China. Section 4 further briefly discusses the possible physical mechanisms related to the differences in the simulations of BCC_CSM1.1 m model and BCC_CSM1.1 model. Finally, section 5 provides the conclusions and discussions.

2. Model, Data, and Methodology

2.1. Model

Two versions of BCC_CSM model with coarse resolution (T42 or approximately 280 km; BCC_CSM1.1) and moderate resolution (T106 or approximately 110 km; BCC_CSM1.1 m) [*Wu et al*., 2014], in which the ocean, land surface, atmosphere, and sea ice components are fully coupled, are used in current study. Both models have the same 26 vertical layers in atmosphere. In each version of BCC_CSM model, the atmospheric and land surface component models have the same horizontal resolution (T42 in BCC_CSM1.1 model or T106 in BCC_CSM1.1 m model). The ocean and sea ice component models in both versions of BCC_CSM model have the same horizontal resolution of 1° × 1° poleward of 30–30°S gradually descending to 0.33° between 30°N and 30°S. More details can be found in our previous studies [*Kan et al*., 2015]. As a whole, except for different horizontal resolutions in the atmospheric and land surface component models, both versions of BCC_CSM model adopt the same physical package [*Wu et al*., 2014] as follows: the land surface model BCC_AVIM1.0, the global ocean circulation model MOM4_L40v1, the global dynamic/thermodynamic sea ice model Sea Ice Simulator, the modified deep convection scheme [*Wu*, 2012], dry adiabatic adjustment scheme [*Yan*, 1987], turbulent fluxes over ocean surface calculated by the bulk formulas suggested by *Zeng et al.* [1998] and *Collins et al.* [2006] considering the impacts of waves and sea spray [*Wu et al*., 2010], the radiative transfer, and planet boundary layer schemes which are the same as in Community Atmosphere Model version 3 (CAM3) [*Huang et al*., 2013].

2.2. Data

1. The daily-observed precipitation data from 824 stations (Figure 1) over China during 1960 to 2012, which is collected and quality controlled by the National Meteorological Information Center of the China Meteorological Administration (http://data.cma.cn/data/detail/dataCode/SURF_CLI_CHN_MUL_DAY_V3.0.html).
2. The reanalysis data from National Centers for Environmental Prediction (NCEP)/National Center for Atmospheric Research (NCAR) [*Kalnay et al*., 1996], including daily air temperature, geopotential height, and wind vectors with the horizontal resolution of 2.5° × 2.5° at 17 vertical layers during 1960 to 2012, which are available at ftp://ftp.cdc.noaa.gov/Datasets/ncep.reanalysis.derived/pressure/.
3. The daily precipitation and atmospheric variable outputs of CMIP5 historical experiment simulated by BCC_CSM1.1 and BCC_CSM1.1 m during 1960–2012, which can be downloaded from the website http://adm07.cmcc.it/esgf-web-fe/live.

2.3. Methodology

In current study, we mainly focus on evaluating the model performance over eastern China (east of 105°E; as shown in Figure 1), which is dominated by monsoonal climate [*Ding and Chan*, 2005]. To give details of model performance in different regions of eastern China, which is divided into three subregions (Figure 1) with the consideration of the observed spatiotemporal distribution of precipitation and the climates over these regions dominated by different components of eastern Asian monsoon [*Wang et al*., 2004; *Ding and Chan*, 2005; *Liu et al*., 2005; *Zhu et al*., 2011]. The three subregions shown in Figure 1 are as follows: southern China (Reg1; 20–30°N, 105–122°E), Jianghuai-northern China (Reg2; 30–40°N, 105–122°E), and northeastern

China (Reg3; 40–50°N, 105–135°E). To facilitate the comparison of the modeled and observed precipitation, the observed and modeled precipitation were interpolated onto 1° latitude × 1° longitude grid using the inverse distance weighting method [*Bartier and Keller*, 1996].

To quantitatively evaluate the performance of the two versions of BCC_CSM model in simulating both the precipitation amplitude and pattern of variability simultaneously, the Taylor score S [*Taylor*, 2001] is calculated according to the formula as follows:

$$S = \frac{4(1+R)}{(\sigma + {}^{1}/_{\sigma})^2(1+R_0)} \tag{1}$$

where σ is the simulated spatial standard deviation normalized by that of observation. R is the pattern correlation between observation and simulation, and R_0 is an achievable maximum correlation (here set as 1). It is obvious that higher S indicates better model performance [*Kan et al*., 2015; *Seo et al*., 2013].

Many previous studies indicate that the South China Sea monsoon (SCSM) is a component of the East Asian monsoon and closely related to precipitation and rainy seasons over eastern China [*Tao and Chen*, 1987; *Lau and Yang*, 1997; *Ding and Chan*, 2005]. Based on *Li et al.* [2011], the SCSM index (SCSMI) is given by

$$\mathrm{SCSMI}_i = V_i \Big/ \left[\frac{1}{N}\sum_{i=1}^{N}(V_i)^2\right]^{1/2} \quad (\mathrm{i} = 1, 2, \ldots .\mathrm{N}) \tag{2}$$

where $V_i = \left(\frac{u_i + v_i}{\sqrt{2}}\right)$, u_i and v_i are the 850 hPa zonal and meridional winds regionally averaged over the domain (110–125°E, 10–20°N) at the ith pentad of a year and N is the sample number (the total pentads in a year). We can obtain the SCSMI at each pentad based on equation (2). It is obvious that the negative (positive) SCSMI reflects winter (summer) monsoon characterized by northeasterly (southwesterly) winds [*Li et al*., 2011]. And the date when the SCSMI changes from negative to positive indicates the onset of South China Sea summer monsoon (SCSSM).

The land-sea thermal contrast (LSTC) is the main factor affecting subtropical East Asian monsoon (SEAM), so an index of LSTC (ILSTC), which was first defined by *Sun et al.* [2002] and then further improved by *Huang et al.* [2007], is used to represent both the zonal and meridional LSTCs over eastern China and surrounding oceans. ILSTC is given by

$$\mathrm{ILSTC} = (T_{L1} - T_{O1}) \times \frac{4}{7} + (T_{L2} - T_{O2}) \times \frac{3}{7} \tag{3}$$

where T_{L1} and T_{L2} are the mean air temperature between 850 hPa and 200 hPa levels regionally averaged over land region (20–35°N, 105–120°E) and land region (20–27°N, 105–120°E), respectively. The T_{O1} and T_{O2} are the mean air temperature between over 850 hPa and 200 hPa regionally averaged over ocean area (15–30°N, 120–140°E) and ocean area (5–20°N, 105–120°E), respectively. Therefore, the zonal and meridional LSTCs are indicated by $(T_{L1} - T_{O1})$ and $(T_{L2} - T_{O2})$, respectively. To consider the relative importance, the weighting coefficients 4/7 and 3/7 are adopted for the zonal and meridional LSTCs, respectively. The ILSTC shows a close correlation of 0.92 with the SEAM index, and it can well reflect the variation of SEAM [*Huang et al*., 2007]. It is clear that positive (negative) ILSTC indicates summer (winter) SEAM and large absolute value of ILSTC means strong monsoon.

In addition, the seasonal transition of western Pacific subtropical high (WPSH) is closely related to the onset and withdrawal of the subtropical East Asian summer monsoon (SEASM) and the spatial distribution of precipitation over eastern China in the rainy seasons. The abrupt northward movement of WPSH is accompanied by abrupt changes in the circulation patterns over the East Asian monsoon area, which plays an important role in the precipitation distribution [*Zhou et al*., 2009]. Many indices can be defined to characterize different features of WPSH, such as WPSH area, intensity, and ridge indices. In this study, WPSH ridge index is used to represent the northward movement of WPSH, which is closely with the seasonal shift of the rainfall bands over eastern China [*Zhou et al*., 2009]. Following *Liu and Wu* [2004] and *Li et al.* [2012], the WPSH ridge is where the winds with an easterly component reverse to those with a westerly component, or it is mathematically expressed by $u = 0$ and $\frac{\partial u}{\partial y} > 0$, where u is the 500 hPa zonal wind component. The WPSH ridge index is defined as the latitude of the WPSH ridge regionally averaged over the region bounded by 110–150°E and 10–40°N.

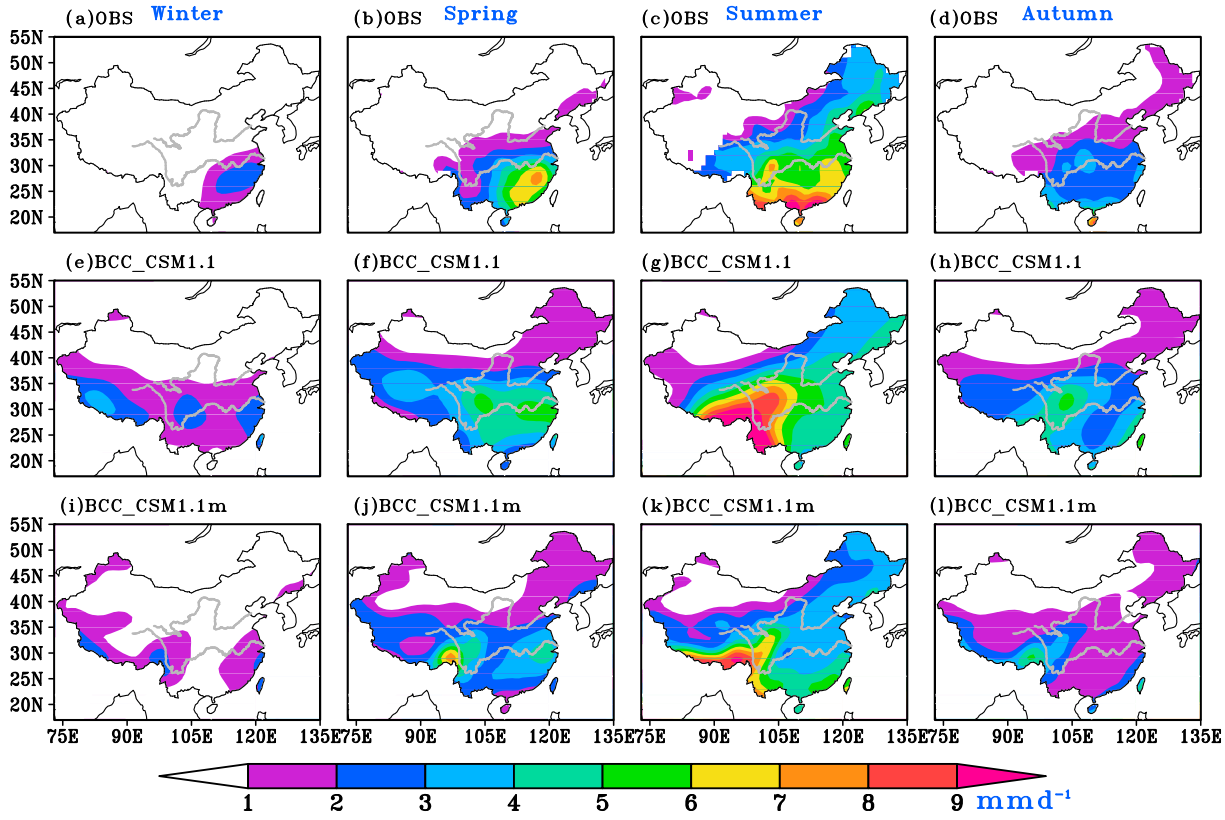

Figure 2. (a–l) Spatial distributions of the observed and modeled seasonal mean precipitation amount averaged over 1960–2012.

3. Results

3.1. Seasonal Variation of Precipitation

Figure 2 gives the spatial distributions of climatic mean precipitation in different seasons from the model simulation and observation over 1960 to 2012. The observed precipitation over China shown in Figures 2a–2d displays distinct seasonal variations: the precipitation increases from winter to summer and then decreases in autumn. Meanwhile, it is also noted that rainband is mainly located to the east of 95°E with the precipitation decreasing from southeastern China to northwestern China in each season. However, in different seasons the spatial distributions of large rainfall centers are quite different. A strong rainfall center over 2 mm d^{-1} in winter (4 mm d^{-1} in spring) is located in the region south to the lower valley of Yangtze River (southeastern China). Two large rainfall centers over 8 mm d^{-1} in summer are located in southern China and Sichuan basin. A strong rainfall center over 5 mm d^{-1} in autumn is found in Hainan Province. Compared to the observation, both BCC_CSM1.1 model (Figures 2e–2h) and BCC_CSM1.1 m model (Figures 2i–2l) can simulate the overall spatiotemporal distributions of precipitation but produce a false strong precipitation center over eastern Tibetan Plateau in each season. This false rainfall center is significantly reduced by BCC_CSM1.1 m in summer and autumn compared with BCC_CSM1.1, indicating that increasing horizontal resolution can improve the simulation of precipitation over eastern Tibetan Plateau characterized by complex terrains [*Kan et al.*, 2015]. In addition, the locations of strong precipitation centers over eastern China simulated by both models are farther north in most seasons compared with the observation.

Figure 3 shows the time-latitude distribution of climatic mean of the simulated and observed precipitation over 1960–2012 averaged along 105–135°E. From the observation (Figure 3c), with the stepwise northward and northeastward advance of the East Asian summer monsoon [*Ding and Chan*, 2005], the monsoonal rainfall band marches northward from the region bounded by 20–25°N to the area of 25–35°N during the period of the 30th–40th pentad; the annual maximal precipitation with the intensity above 3 mm d^{-1} over northeastern China (40–50°N) appears in the period between the 40th and the 45th pentad. After the 50th pentad, the rainfall band rapidly moves southward from northeastern China to the southern China due to the retreat

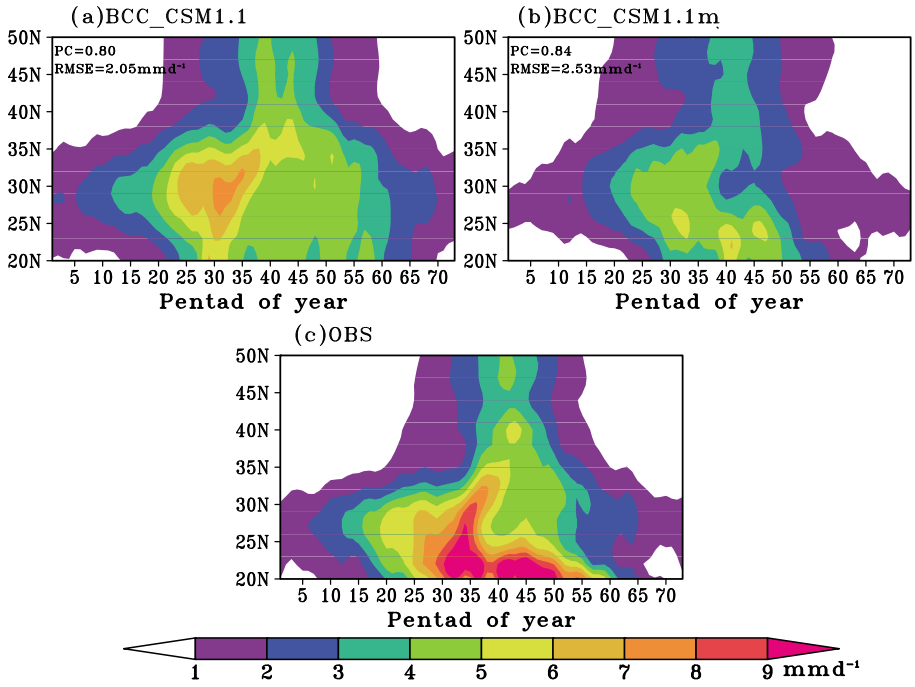

Figure 3. (a–c) The time-latitude distributions of modeled and observed pentad climatic mean precipitation over 1960–2012 averaged along 105–135°E.

of the summer monsoon [*Ding and Chan*, 2005]. Both BCC_CSM1.1 (Figure 3a) and BCC_CSM1.1 m (Figure 3b) can basically reproduce the seasonal shifts of the rainfall band over eastern China. The pattern correlation produced by BCC_CSM1.1 m model is 0.84, which is slightly larger than that produced by BCC_CSM1.1 model, indicating that BCC_CSM1.1 m model with fine horizontal resolution improves the seasonal shifts of the rainfall band over eastern China. However, BCC_CSM1.1 m model produces relatively larger root-mean-square error (RMSE) than BCC_CSM1.1 model (2.53 mm d^{-1} versus 2.05 mm d^{-1}).

Figure 4 gives the seasonal variation of modeled and observed pentad climatic mean precipitation during 1960–2012, regionally averaged over each subregion of eastern China. As shown in Figure 4a, the observed precipitation over southern China shows two annual peaks corresponding to the presummer and second rainy seasons in southern China [*Tao and Chen*, 1987; *Ding*, 1992; *Ding and Chan*, 2005]: relatively strong one over 9 mm d^{-1} around the 34th pentad and a weak one above 7 mm d^{-1} near the 45th pentad. BCC_CSM1.1 model produces only one precipitation annual peak over southern China and fails to simulate the secondary peak. It is obvious that the modeled precipitation annual peak in BCC_CSM 1.1 model appears at the 31st pentad, which is about 2 pentads earlier than the observation. Meanwhile, BCC_CSM1.1 model underestimates (overestimates) the precipitation over southern China during the 15th–52nd pentad (1st–14th pentad and 53rd–73rd pentad) compared to the observation. Comparing with BCC_CSM1.1 model, BCC_CSM1.1 m model well simulates the two precipitation annual peaks over southern China and their occurrence time. However, BCC_CSM1.1 m model underestimates the precipitation in most time of year (Figure 4a).

As shown in Figure 4b, the observed precipitation over Jianghuai-northern China steadily increases from winter to middle summer and then decreases from middle summer to winter. It is also noted that the precipitation sharply increases from 3 mm d^{-1} in the 34th pentad to 6 mm d^{-1} in the 38th pentad during a short period. The annual maximum of precipitation over 5 mm d^{-1} appears around the 37th pentad, corresponding to the Meiyu and northern China rainy seasons [*Ding and Chan*, 2005]. Both versions of BCC_CSM model well reproduced the overall features of the annual variation of the precipitation with good agreements in the annual peak and its occurrence time with the observation. It is also shown that BCC_CSM1.1 model produced a false secondary peak during the 25th–30th pentad and overestimated the precipitation over Jianghuai-northern China in most time of a year with large biases during the 20th to

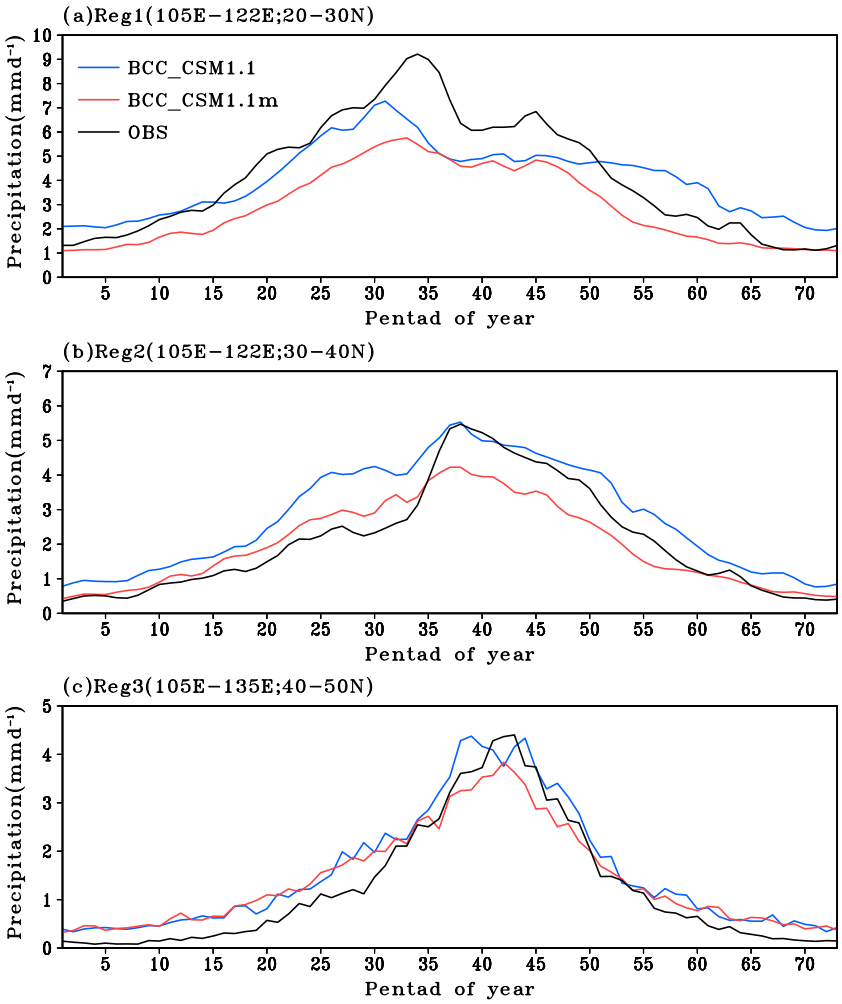

Figure 4. (a–c) Seasonal variation of modeled and observed pentad climatic mean precipitation during 1960–2012 regionally averaged over each subregion of eastern China.

33rd pentad. Despite that the precipitation annual peak produced by BCC_CSM1.1 m model is much weaker than the observation, the precipitation simulated by BCC_CSM1.1 m model shows better agreement with the observation during the 1st–35th pentad and the 58th–73rd pentad than that from BCC_CSM1.1 model. However, the precipitation simulated by BCC_CSM1.1 m model is underestimated by 1–2 mm d^{-1} during middle to late summer (36th to 48th pentad), leading to underestimation of the summer precipitation over Jianghuai-northern China [*Kan et al.*, 2015].

As shown in Figure 4c, the observed precipitation over northeastern China exhibits a distinct annual peak over 4 mm d^{-1} around the 42nd pentad, corresponding to the rainy season in northeastern China [*Ding and Chan*, 2005]. Both versions of BCC_CSM model well reproduced the overall features of the precipitation seasonal variation over northeastern China. The occurrence time of the precipitation annual peak in BCC_CSM1.1 model is about three pentads earlier than the observation. The BCC_CSM1.1 m model realistically reproduced the occurrence time of the precipitation annual peak over northeastern China except for the intensity slightly underestimated. In addition, the precipitation over northeastern China is overestimated by BCC_CSM1.1 model in most time of a year. Despite that BCC_CSM1.1 m model much more underestimated the precipitation over northeastern China during middle to late summer (36th to 48th pentad) relative to BCC_CSM1.1 model, biases of the modeled precipitation are smaller in BCC_CSM1.1 m than in BCC_CSM1.1 model during the 1st–35th pentad and the 50th–72nd pentad.

Overall, both versions of BCC_CSM model can well simulate the basic features of precipitation seasonal cycle over each subregion of eastern China. Some obvious biases can be noted, i.e., earlier occurrence time of the

precipitation annual peak over southern China and northeastern China in BCC_CSM1.1 and large negative biases in the BCC_CSM1.1 m modeled precipitation over southern China (Jianghuai-northern China and northeastern China) during spring to autumn (middle to late summer). As a whole, BCC_CSM1.1 m model with finer horizontal resolution tends to show better performance in simulating the timing and intensity of precipitation during dry seasons over eastern China except for larger biases in the quantity during rainy seasons relative to BCC_CSM1.1 model. Meanwhile, the occurrence time of the annual peak of precipitation over each subregion of eastern China is much more accurately simulated in BCC_CSM1.1 m model than in BCC_CSM1.1 model.

3.2. Quantitative Evaluation

Figure 5 displays the differences in the seasonal mean precipitation over eastern China between BCC_CSM1.1 simulation and observation and those between BCC_CSM1.1 m simulation and BCC_CSM1.1 simulation. The precipitation over southern China (the other regions of eastern China) in winter and spring is underestimated (overestimated) by BCC_CSM1.1 model (Figures 5a and 5b) with relatively large biases over the upper valleys of Yangtze River and Huanghe River. Meanwhile, the BCC_CSM1.1 model overestimated (underestimated) the precipitation over southern China, Jianghuai Valley, and central to southern northeastern China (the other regions of eastern China) during summer (Figure 5c). In autumn, the precipitation over most part of eastern China is overestimated by BCC_CSM1.1 model (Figure 5d). Compared with BCC_CSM1.1 model, BCC_CSM1.1 m model largely reduced (increased) the biases over the region bounded by 28–40°N (southern China and northeastern China) in winter and spring (Figures 5e and 5f), although the positive precipitation biases over eastern China in summer produced by BCC_CSM1.1 model are significantly reduced by BCC_CSM1.1 m model, which strengthened the negative precipitation biases over most southeastern China (Figure 5g). In addition, the BCC_CSM1.1 m model reduced the positive precipitation biases in autumn of the BCC_CSM1.1 simulation over almost entire eastern China (Figure 5h).

The skill score *S* is further used to quantitatively evaluate the model performance in simulating the precipitation amplitude and pattern of variability over the three subregions of eastern China. As shown in Figure 6, both models' performance in simulating the precipitation over each subregion of eastern China exhibits obvious seasonal variation. The score of the BCC_CSM1.1 model in simulating the precipitation over southern China (Figure 6a) ranges from 0 to 0.6, with relatively larger values of *S* in winter and spring than in summer and autumn; it is obvious that the BCC_CSM1.1 m model with finer horizontal resolution shows better ability in simulating the precipitation over southern China than BCC_CSM1.1 model in most pentads with much larger improvements during late summer and autumn (40th–65th pentad). Figure 6b shows that BCC_CSM1.1 model exhibits very good (relatively bad) performance with the *S* over 0.8 (below 0.6) in simulating the precipitation over Jianghuai-northern China in most time of a year (middle summer). Compared to BCC_CSM1.1 model, BCC_CSM1.1 m model shows worse ability in simulating the precipitation amplitude and pattern of variability over Jianghuai-northern China in almost all pentads of a year. From Figure 6c, BCC_CSM1.1 model shows relatively worse ability in simulating the precipitation over northeastern China in winter and late summer compared with the other seasons. Relative to BCC_CSM1.1 model, BCC_CSM1.1 m model exhibits comparable skill in winter and autumn with slight improvements during the 21st–45th pentad over northeastern China.

Overall, the performance of both versions of BCC_CSM model in simulating the precipitation over eastern China vary regionally and seasonally. Compared to BCC_CSM1.1 model, BCC_CSM1.1 m model shows improvement (deterioration) in the simulation of precipitation amplitude and pattern of variability over southern China (Jianghuai-northern China) in most time of a year. For northeastern China, BCC_CSM1.1 m model with finer horizontal resolution shows comparable performance to BCC_CSM1.1 model in simulating the precipitation amplitude and pattern of variability during winter and autumn with slightly better ability during middle spring to late summer.

4. Possible Causes

As the results mentioned above, compared with BCC_CSM1.1 model, despite that some deterioration of the precipitation in quantity from BCC_CSM1.1 m model can be noted over eastern China during rainy seasons, BCC_CSM1.1 m with much finer horizontal resolution improves the simulation of the precipitation seasonal

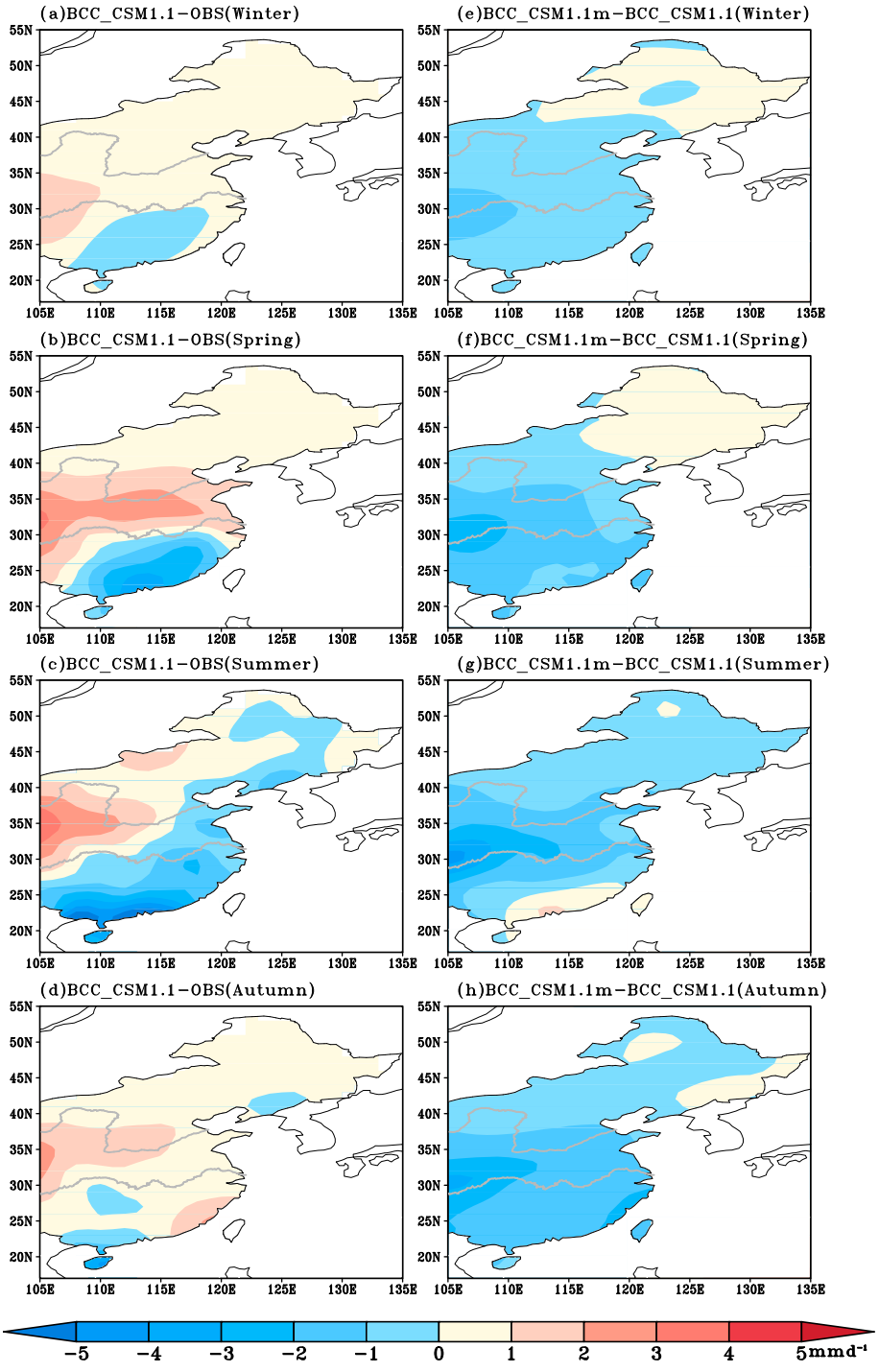

Figure 5. (a–h) Spatial distributions of the differences in the seasonal mean precipitation averaged over 1960–2012.

variation and occurrence time of precipitation annual peaks over different subregions of eastern China, which is closely associated with the seasonal transition of East Asian monsoon [*Ding and Chan*, 2005].

To illustrate the mechanisms related to these improvements or deterioration in BCC_CSM1.1 m model relative to BCC_CSM1.1 model, Figure 7 first gives the time-latitude distributions of the pentad climatic mean wind field at 850 hPa level over 1960–2012 averaged along 110–125°E in the simulations of the two models and NCEP reanalysis data. As shown in the NCEP reanalysis data (Figure 7c), over the low

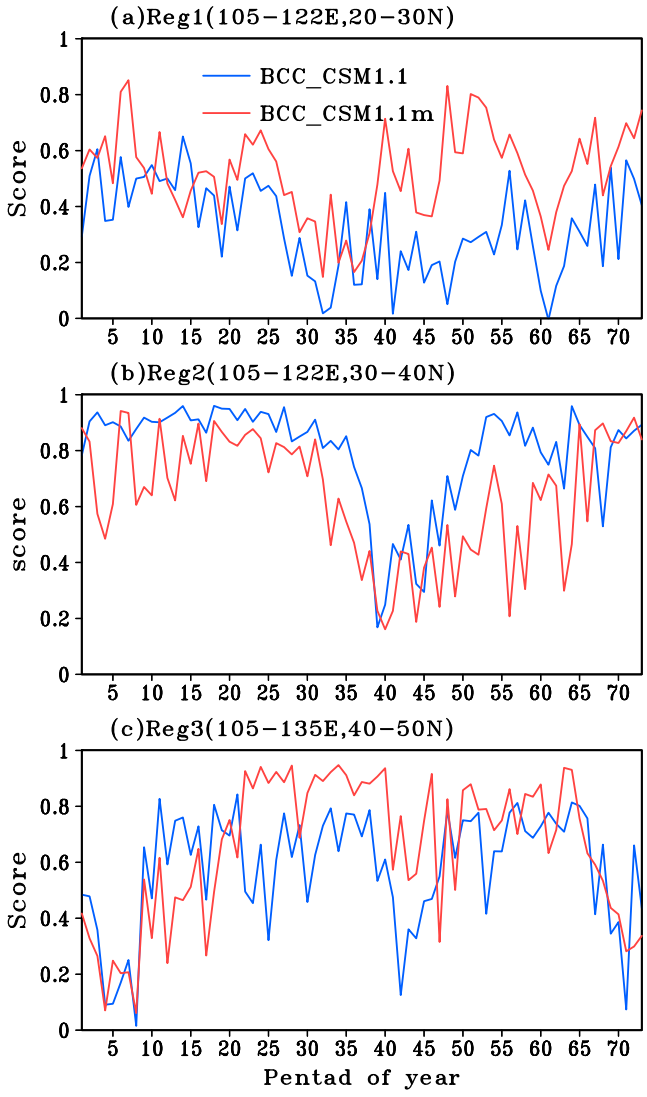

Figure 6. (a–c) Seasonal variation for the scores of BCC_CSM1.1 and BCC_CSM1.1 m in simulating the pentad climatic mean precipitation over 1960–2012 in each subregion of eastern China.

latitudes between 5°N and 20°N, northeasterly winds prevail during cold seasons (1st–25th pentad and 60th–72nd pentad) and southwesterly winds are pronounced during warm seasons (28th–55th pentad), which are corresponding to the winter and summer monsoons. The first appearance of the southwesterly winds over the regions south to 20°N, indicating the onset of the summer monsoon, takes place around the 28th pentad and then expand northward to the areas north to 25°N with the wind speed strengthened during the 35th to 45th pentad. The southwesterly winds reach the northernmost position of 50°N around the 50th pentad and then change to northwesterly winds. These features are corresponding to the seasonal movements of the East Asian monsoon [*Ding and Chan*, 2005], which lead to the seasonal shifts of the rainband over eastern China (Figure 3). As shown in Figure 7a, the BCC_CSM1.1 model produces comparable features in the 850 hPa winds with NCEP data, but the southwesterly winds over the area between 10°N and 20°N first appear around the 26th pentad, which is about 2 pentads earlier than the NCEP data. From Figure 7b, despite that the 850 hPa southwesterly winds at higher latitudes in summer simulated by BCC_CSM1.1 m model with finer horizontal resolution are much weaker than NCEP data and BCC_CSM1.1 simulation, the seasonal variation of the winds at 850 hPa over the regions south to 20°N and the northward expansion of southwesterly winds are realistically simulated, especially that the first appearance of the 850 hPa southwesterly winds over the region between 10°N and 20°N in BCC_CSM1.1 m model happens around the 28th pentad, which is in good agreement with the NCEP data, indicating that the earlier onset of the summer monsoon in BCC_CSM1.1 model is improved by the increase of model horizontal resolution. However, it is also noted that BCC_CSM1.1 m model produces false southeasterly winds between 25°N and 35°N during middle to late summer (the 38th–45th pentad), which are resulted from the much stronger WPSH with farther northwest position than NCEP data and simulations of BCC_CSM1.1 model [*Kan et al.*, 2015], leading to much weaker southwesterly winds at 850 hPa and northeastward water vapor transport (Figure 8) and thereafter less precipitation over most regions of eastern China than the observation and BCC_CSM1.1 simulation in summer (Figures 4 and 5c).

The climates over eastern China are largely affected by the East Asian monsoon system [*Ding and Chan*, 2005; *Liu et al.*, 2005; *Li et al.*, 2010; *Zhu et al.*, 2011], which includes two components: tropical monsoon (i.e., SCSM) and subtropical monsoon [*Wang et al.*, 2004]. Many previous studies have suggested that the onset of SCSSM is a precursor to the East Asian summer monsoon (EASM) development and start of the rainy seasons over

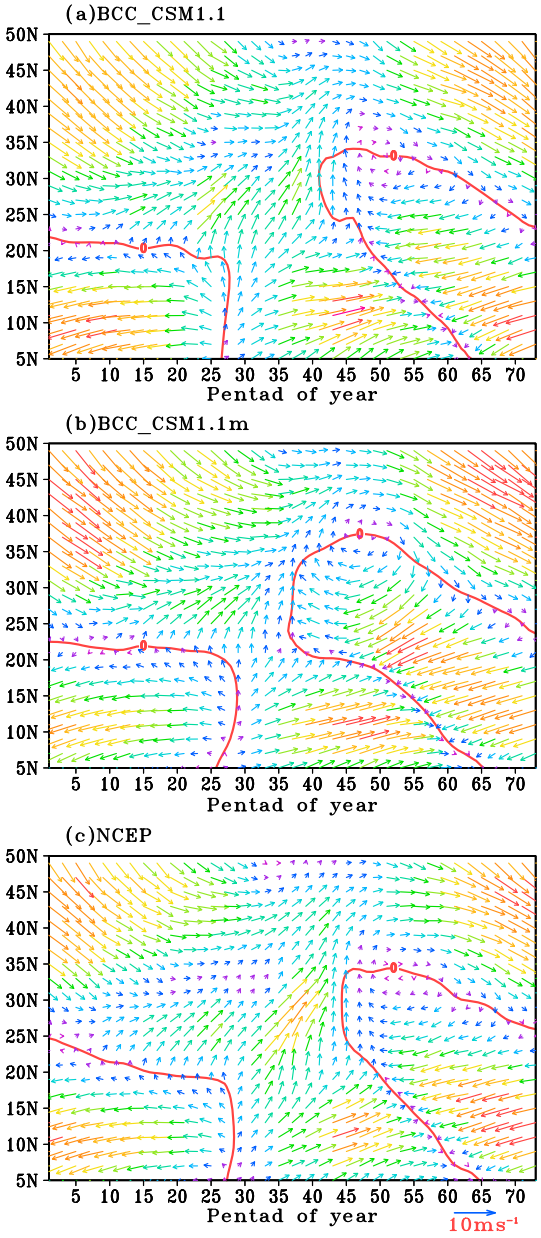

Figure 7. (a–c) The time-latitude distributions of the pentad climatic mean 850 hPa wind vector over 1960–2012 averaged along 110–125°E from model simulation and NCEP reanalysis data. The red contour lines indicate the zonal wind $u = 0$.

eastern China [*Lau and Yang*, 1997; *Wang et al.*, 2004]. The seasonal transition features of the SCSM from model simulation and NCEP reanalysis are exhibited in Figure 9a. It is clear that the SCSSM bursts in late May (around the 28th pentad); this is consistent with the previous studies [*Li et al.*, 2011; *Kajikawa and Wang*, 2012]. Both BCC_CSM1.1 model and BCC_CSM1.1 m model can reproduce the basic seasonal transition features of SCSM. However, the onset date of the SCSSM simulated by BCC_CSM1.1 model is about three pentads earlier than that of NCEP reanalysis. Compared to BCC_CSM1.1 model, BCC_CSM1.1 m model simulates the onset date of SCSSM much more precisely and leads to more accurate simulation of the occurrence time of the precipitation annual peak over southern China.

Some earlier studies indicate that the rainy season in southern China first starts in middle to late May marked by the onset of SCSSM [*Wang et al.*, 2004] and the northward movement of rain belts well corresponds to the stepwise northward and northeastward advance of the subtropical East Asian summer monsoon (SEASM) and WPSH [*Ding and Chan*, 2005; *Zhou et al.*, 2009]. Figure 9b shows the seasonal variation of the LSTC, which represents the SEAM [*Huang et al.*, 2007] from the model simulation and NCEP reanalysis. From the ILSTC in the NCEP reanalysis, it is noted that the SEASM bursts in early June, which is about four pentads later than the onset date of SCSSM. Both models can well reproduce that the onset date of SEASM is later than that of SCSSM. Meanwhile, the onset date of SEASM produced by BCC_CSM1.1 model is about three to four pentads earlier than that in the NCEP reanalysis, which may correspond to the precipitation annual peak over Jianghuai-northern China falsely simulated during the 25th–30th pentad (Figure 4b). BCC_CSM1.1 m model well produced the onset date of SEASM, resulting in the accurate simulation of the occurrence time of the precipitation annual peak over Jianghuai-northern China.

As shown in Figures 9a and 9b, the BCC_CSM1.1 model produced earlier onsets of the SCSSM and SEASM relative to NCEP reanalysis, leading to earlier starts of the rainy seasons and earlier occurrence time of the precipitation annual peak over each subregion in eastern China (Figure 4) than the observation. However, the BCC_CSM1.1 m model well simulated the onsets of both SCSSM and SEASM, leading to much better agreements with the timing of the observed precipitation over each subregion of eastern China compared

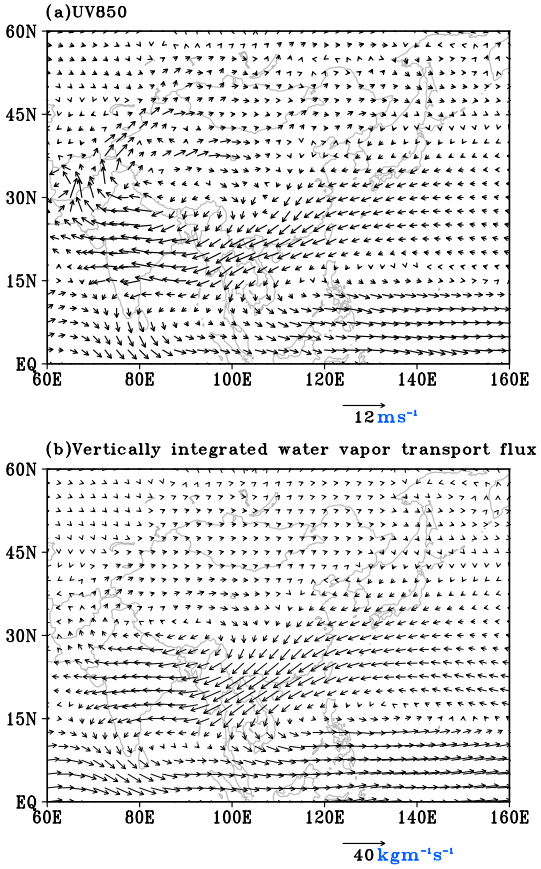

Figure 8. (a) Differences in the summer mean 850 hPa wind vector and (b) vertically integrated (surface to 300 hPa) water vapor transport flux between BCC_CSM1.1 m and BCC_CSM1.1 averaged over 1960–2012.

to BCC_CSM1.1 model (Figure 4). Meanwhile, it is also noted that the precipitation during rainy season over each subregion in eastern China is much more underestimated by BCC_CSM1.1 m model compared to BCC_CSM1.1 model (Figures 4 and 5). To indicate the reasons related to the biases in the simulated precipitation during rainy season, Figure 9c further gives the seasonal variation of the WPSH ridge from NCEP reanalysis and model simulation. Both simulation and NCEP reanalysis show that the WPSH ridge moves northward (southward) during winter to summer (summer to winter) with the northmost location in late summer, showing a very obvious seasonal shift. In addition, the northward jump of WPSH to the north of 20°N in BCC_CSM1.1 model is about two to three pentads earlier than the NCEP reanalysis and BCC_CSM1.1 m model simulation, leading to the earlier start of the rainy seasons over eastern China. It is also noted that BCC_CSM1.1 m model produced much weaker LSTC (Figure 9b) in summer compared to BCC_CSM1.1 model, which is well corresponding to the larger positive differences of the simulated upward net surface heat flux in summer between BCC_CSM1.1 m and BCC_CSM1.1 over South China Sea and northwest Pacific than over the land regions of southeastern China [*Kan et al.*, 2015]. The weaker LSTC (Figure 9b) and much stronger WPSH with farther northwest position result in much weaker southwesterly winds at 850 hPa level and less northeastward water vapor transport (Figure 8) and thereafter much more underestimated precipitation (Figures 4 and 5) over eastern China during summer in BCC_CSM1.1 m than in BCC_CSM1.1 model.

5. Concluding Remarks and Discussions

The ability of the two versions of BCC_CSM (BCC_CSM1.1 and BCC_CSM1.1 m) with two horizontal resolutions in simulating the seasonal cycle of precipitation over eastern China has been evaluated. The possible causes related to the model biases and underlying physical mechanisms are also further revealed and discussed. Main findings in current study are shown as follows.

Both versions of BCC_CSM model can well produce the basic features of the precipitation seasonal cycle over eastern China. However, the occurrence time of the precipitation annual peak over eastern China simulated by BCC_CSM1.1 with coarse horizontal resolution is earlier than the observation. BCC_CSM1.1 m model largely underestimated the precipitation over southern China (Jianghuai-northern China and northeastern China) in spring to autumn (middle to late summer). Overall, BCC_CSM1.1 m model with finer resolution tends to show better performance in simulating the timing and amount of precipitation over eastern China during dry seasons except for larger biases in rainy seasons compared to BCC_CSM1.1 model. Furthermore, BCC_CSM1.1 m exhibits higher accuracy in simulating the occurrence time of the annual peak of precipitation over each subregion of eastern China than BCC_CSM1.1 model.

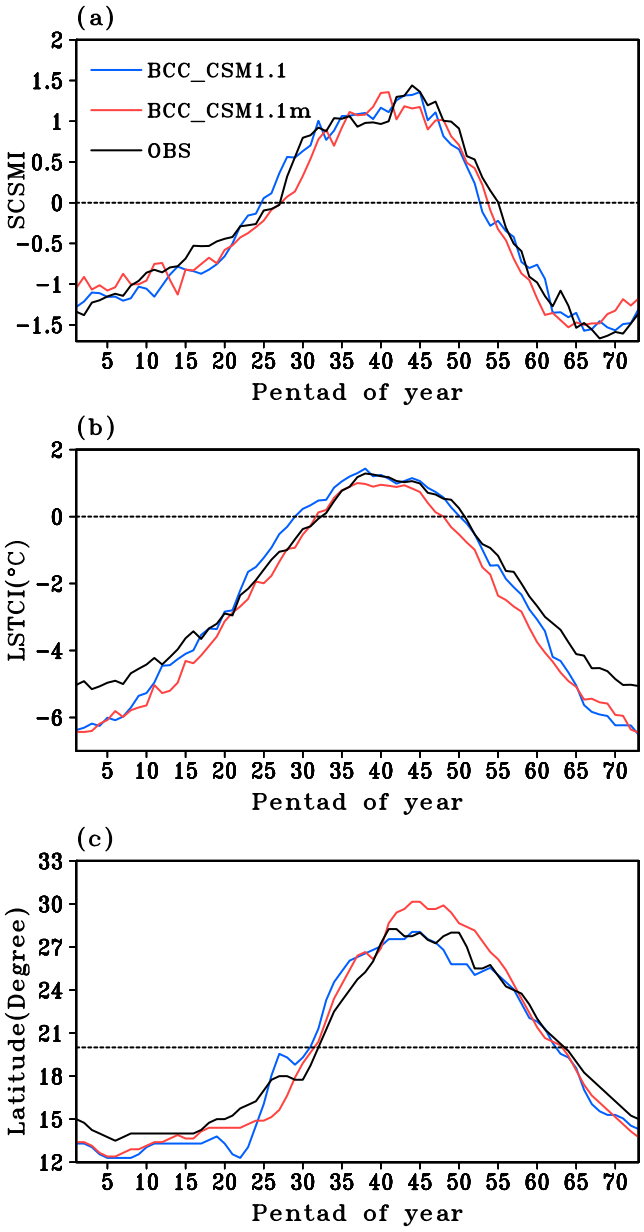

Figure 9. Seasonal variations of the pentad climatic mean (a) SCSMI, (b) ILSTC, and (c) latitudes of the western Pacific subtropical high ridge line over 1960–2012 from model simulations and NCEP reanalysis data.

Quantitative evaluation of the skill in simulating the precipitation amplitude and pattern of variability indicates that the performance of both versions of BCC_CSM model vary regionally and seasonally. Relative to BCC_CSM1.1 model, BCC_CSM1.1 model with finer horizontal resolution shows improvements (deterioration) over southern China (Jianghuai-northern China) in most time of a year and comparable performance over northeastern China during winter and autumn with slightly higher skill during late spring to summer.

Further mechanism analysis suggests that the earlier onsets of the SCSSM and SEASM and northward jump of WPSH in the BCC_CSM1.1 simulation lead to the earlier start of the rainy seasons and occurrence time of the precipitation annual peaks over different subregions of eastern China compared to the observation and BCC_CSM1.1 m simulation. The seasonal variation of precipitation and the occurrence time of the precipitation annual peaks over different subregions of eastern China are better simulated by BCC_CSM1.1 m model relative to BCC_CSM1.1 model; this can be related to the more accurately simulated onsets of SCSSM and SEASM and northward jump of WPSH in BCC_CSM1.1 m model. However, BCC_CSM1.1 m model produced much stronger WPSH with farther northwest position and weaker LSTC than BCC_CSM1.1 model in summer, resulting in much underestimated northeastward water vapor transport and summer precipitation over most eastern China.

Current study shows that increase of model horizontal resolution does lead to improvements in the seasonal variation of precipitation and occurrence time of the precipitation annual peaks over eastern China; this can be attributed to the much more realistically simulated seasonal shifts of the East Asian monsoon and WPSH in BCC_CSM1.1 m model with finer horizontal resolution than in BCC_CSM1.1 model. Similar results were obtained by *Li et al.* [2015], who have shown that the seasonal variation of rainfall over East Asia arising from the onset and advancement of the Asian monsoon is improved by increasing the horizontal resolution of NCAR CAM5 model. This is encouraging and favorable for the operational seasonal climate forecasts over eastern China by using the BCC_CSM model with high horizontal resolution. However, relative to BCC_CSM1.1 model, BCC_CSM1.1 m model tends to produce much stronger WPSH with farther northwest position and weaker LSTC in summer, leading to much weaker northeastward water vapor transport and less

summer precipitation over most eastern China. The summer precipitation over eastern China is largely attributed to the convective precipitation, which is one of the important features of EASM [*Huang et al*., 2015; *Kan et al*., 2015]. The large-scale temperature field is significantly affected by the diabatic heating due to convection, leading to the changes in the monsoonal circulation and thereafter precipitation [*Ose*, 1998]. The summer precipitation especially convective precipitation is largely affected by resolution through the model physics and dynamics rather than through the description of topographical detail [*Giorgi and Marinucci*, 1996; *Tang et al*., 2007]. Increase of horizontal resolution tends to result in more large-scale and less convective precipitation simulation [*Duffy et al*., 2003; *Kan et al*., 2015]. *Iorio et al.* [2004] found the improved precipitation simulation by increasing model horizontal resolution during winter and fall when precipitation is mainly resulted from the resolved scheme (e.g., large-scale precipitation) rather than the convective parameterization (e.g., convective precipitation). However, fewer improvements can be seen during spring and summer when the convective scheme dominates. This can be reinforced by the findings of *Kan et al.* [2015], which show that the summer convective precipitation is significantly reduced in BCC_CSM1.1 m model compared to BCC_CSM1.1 model due to more cloud processes determined by the resolved schemes rather than convection scheme by increasing horizontal resolution. *Jung et al.* [2012] found that the majority of the improvements by increasing horizontal resolution arise from the step from T159 to T511 with few changes for further resolution increases to T1279 and T2047. Therefore, to improve the summer precipitation simulation over eastern China in BCC_CSM model, only increasing the model horizontal resolution is not enough, further improving the model dynamics (e.g., vertical resolution), physical parameterizations (e.g., convective and cloud microphysics schemes), and model tuning (e.g., retuning the parameter values in different subgrid-scale physical processes to optimum values at each resolution) should be conducted [*Pope and Stratton*, 2002; *Duffy et al*., 2003; *Iorio et al*., 2004; *Roeckner et al*., 2006; *Rauscher et al*., 2010], with the model horizontal resolution increased in the future.

Acknowledgments

This work was supported by the National Natural Science Foundation of China, the major special cultivation project of the Qinghai Tibet Plateau under grant 91537102, the Key Project of Chinese National Programs for Research and Development under grant 2016YFA0602104, and the Jiangsu Collaborative Innovation Center for Climate Change. We are grateful to NCEP/NCAR ftp://ftp.cdc.noaa.gov/Datasets/ncep.reanalysis.derived/pressure/) for allowing us to use the reanalysis data. We thank the National Meteorological Information Center of the China Meteorological Administration for providing the gauge-observed precipitation data (http://data.cma.cn/data/detail/dataCode/SURF_CLI_CHN_MUL_DAY_V3.0.html). We also acknowledge the World Climate Research Program's Working Group on Coupled Modeling, which is responsible for CMIP5 making the outputs of BCC_CSM models available at http://adm07.cmcc.it/esgf-web-fe/live. We appreciate the Editor and two anonymous reviewers for their careful review and constructive comments.

References

Bartier, P. M., and C. P. Keller (1996), Multivariate interpolation to incorporate thematic surface data using inverse distance weighting (IDW), *C. R. Geosci.*, *22*(7), 795–799, doi:10.1016/0098-3004(96)00021-0.

Boville, B. A. (1991), Sensitivity of simulated climate to model resolution, *J. Clim.*, *4*(5), 469–485.

Boyle, J. S. (1993), Sensitivity of dynamical quantities to horizontal resolution for a climate simulation using the ECMWF (cycle 33) model, *J. Clim.*, *6*(5), 796–815.

Collins, W. D., P. J. Rasch, B. A. Boville, J. J. Hack, J. R. McCaa, D. L. Williamson, B. P. Briegleb, C. M. Bitz, S.-J. Lin, and M. Zhang (2006), The formulation and atmospheric simulation of the Community Atmosphere Model version 3 (CAM3), *J. Clim.*, *19*, 2144–2161.

Ding, Y., and J. C. Chan (2005), The East Asian summer monsoon: An overview, *Meteorol. Atmos. Phys.*, *89*(1-4), 117–142.

Ding, Y., G. Ren, Z. Zhao, Y. Xu, Y. Luo, Q. Li, and J. Zhang (2007), Detection, causes and projection of climate change over China: An overview of recent progress, *Adv. Atmos. Sci.*, *24*, 954–971.

Ding, Y. H. (1992), Summer monsoon rainfalls in China, *J. Meteorol. Soc. Jpn.*, *70*(1B), 373–396.

Duffy, P. B., B. Govindasamy, J. P. Iorio, J. Milovich, K. R. Sperber, K. E. Taylor, M. F. Wehner, and S. L. Thompson (2003), High-resolution simulations of global climate, Part 1: Present climate, *Clim. Dyn.*, *21*(5-6), 371–390.

Gao, F., X. Xin, and T. Wu (2012), A study of the prediction of regional and global temperature on decadal time scale with BCC_CSM1.1 model (in Chinese), *Chin. J. Atmos. Sci.*, *36*(6), 1165–1179.

Gao, X., Y. Xu, Z. Zhao, J. Pao, and F. Giorgi (2006a), On the role of resolution and topography in the simulation of East Asia precipitation, *Theor. Appl. Climatol.*, *86*, 173–185.

Gao, X., J. S. Pal, and F. Giorgi (2006b), Projected changes in mean and extreme precipitation over the Mediterranean region from a high resolution double nested RCM simulation, *Geophys. Res. Lett.*, *33*, L03706, doi:10.1029/2005GL024954.

Gao, X., Y. Shi, and F. Giorgi (2011), A high resolution simulation of climate change over China, *Sci. China Earth Sci.*, *54*(3), 462–472.

Giorgi, F., and M. R. Marinucci (1996), A investigation of the sensitivity of simulated precipitation to model resolution and its implications for climate studies, *Mon. Weather Rev.*, *124*(1), 148–166.

Giorgi, F., and L. O. Mearns (1991), Approaches to the simulation of regional climate change: A review, *Rev. Geophys.*, *29*, 191–216, doi:10.1029/90RG02636.

Hertwig, E., J. von Storch, D. Handorf, K. Dethloff, I. Fast, and T. Krismer (2015), Effect of horizontal resolution on ECHAM6-AMIP performance, *Clim. Dyn.*, *45*, 185–211.

Huang, A., Y. Zhang, and X. Gao (2007), Impacts of coastal SST variability on the East Asian summer monsoon, *Adv. Atmos. Sci.*, *24*, 259–270.

Huang, A., et al. (2013), Extended range simulations of the extreme snow storms over southern China in early 2008 with the BCC_AGCM2.1 model, *J. Geophys. Res. Atmos.*, *118*, 8253–8273, doi:10.1002/jgrd.50638.

Huang, A., Y. Zhou, Y. Zhang, D. Huang, Y. Zhao, and H. Wu (2014), Changes of the annual precipitation over central Asia in the twenty-first century projected by multimodels of CMIP5, *J. Clim.*, *27*, 6627–6646.

Huang, Y., Y. Zhang, A. Huang, X. Kuang, Y. Yao, D. Huang, and L. Zhang (2015), Analysis of the simulated different-class Meiyu precipitation and associated circulation by the BCC_AGCM2.0.1, *Theor. Appl. Climatol.*, *120*(3-4), 631–641.

Iorio, J. P., P. B. Duffy, B. Govindasamy, S. L. Thompson, M. Khairoutdinov, and D. Randall (2004), Effects of model resolution and sub-grid scale physics on the simulation of precipitation in the continental United States, *Clim. Dyn.*, *23*, 243–258.

Jiang, Y., A. Huang, and H. Wu (2015), Evaluation of the performance of Beijing Climate Center climate system model with different horizontal resolution in simulating the annual surface temperature over central Asia (in Chinese), *Chin. J. Atmos. Sci.*, *39*(3), 535–547.

Jung, T., et al. (2012), High-resolution global climate simulations with the ECMWF model in Project Athena: Experimental design, model climate, and seasonal forecast skill, *J. Clim.*, *25*, 3155–3172.
Kajikawa, Y., and B. Wang (2012), Interdecadal change of the South China Sea summer monsoon onset, *J. Clim.*, *25*, 3207–3218.
Kalnay, E., et al. (1996), The NCEP/NCAR 40-year reanalysis project, *Bull. Am. Meteorol. Soc.*, *77*(3), 437–471.
Kan, M., A. Huang, Y. Zhao, Y. Zhou, B. Yang, and H. Wu (2015), Evaluation of the summer precipitation over China simulated by BCC_CSM model with different horizontal resolutions during the recent half century, *J. Geophys. Res. Atmos.*, *120*, 4657–4670, doi:10.1002/2015JD023131.
Lau, K. M., and S. Yang (1997), Climatology and interannual variability of the Southeast Asian summer monsoon, *Adv. Atmos. Sci.*, *14*(2), 141–162.
Leung, L. R., and Y. Qian (2003), The sensitivity of precipitation and snowpack simulations to model resolution via nesting in regions of complex terrain, *J. Hydrometeorol.*, *4*(6), 1025–1043.
Li, C., T. Li, J. Liang, D. Gu, A. Lin, and B. Zheng (2010), Interdecadal variations of meridional winds in the South China Sea and their relationship with summer climate in China, *J. Clim.*, *23*, 825–841.
Li, C., J. Pan, and Z. Que (2011), Variation of the East Asian monsoon and the tropospheric biennial oscillation, *Chin. Sci. Bull.*, *56*(1), 70–75.
Li, J., R. Yu, W. Yuan, H. Chen, W. Sun, and Y. Zhang (2015), Precipitation over East Asia simulated by NCAR CAM5 at different horizontal resolutions, *J. Adv. Model. Earth Syst.*, *7*, 774–790, doi:10.1002/2014MS000414.
Li, L., W. Li, and Y. Kushnir (2012), Variation of the North Atlantic subtropical high western ridge and its implication to southeastern US summer precipitation, *Clim. Dyn.*, *39*, 1401–1412.
Liu, B., M. Xu, M. Henderson, and Q. Ye (2005), Observed trends of precipitation amount, frequency, and intensity in China, 1960-2000, *J. Geophys. Res.*, *110*, D08103, doi:10.1029/2004JD004864.
Liu, Y., and G. Wu (2004), Progress in the study on the formation of the summertime subtropical anticyclone, *Adv. Atmos. Sci.*, *21*, 322–342.
Marshall, S., J. O. Roads, and R. J. Oglesby (1997), Effects of resolution and physics on precipitation in the NCAR Community Climate Model, *J. Geophys. Res.*, *102*, 19,529–19,541, doi:10.1029/97JD01428.
Mass, C. F., D. Ovens, K. Westrick, and B. A. Colle (2002), Does increasing horizontal resolution produce more skillful forecasts? *Bull. Am. Meteorol. Soc.*, *83*(3), 407–430.
Navarra, A., S. Gualdi, S. Masina, S. Behera, J.-J. Luo, S. Masson, E. Guilyardi, P. Delecluse, and T. Yamagata (2008), Atmospheric horizontal resolution affects tropical climate variability in coupled models, *J. Clim.*, *21*(4), 730–750.
Ning, L., and R. S. Bradley (2016), NAO and PNA influences on winter temperature and precipitation over the eastern United States in CMIP5 GCMs, *Clim. Dyn.*, *46*(3), 1257–1276.
Ose, T. (1998), Seasonal change of Asian summer monsoon circulation and its heat source, *J. Meteorol. Soc. Jpn.*, *76*, 1045–1063.
Pope, V. D., and R. A. Stratton (2002), The processes governing horizontal resolution sensitivity in a climate model, *Clim. Dyn.*, *19*, 211–236.
Rajendran, K., A. Kitoh, and S. Yukimoto (2004), South and East Asian summer monsoon climate and variation in the MRI coupled model (MRI-CGCM2), *J. Clim.*, *17*, 763–782.
Ramu, D. A., C. T. Sabeerali, R. Chattopadhyay, D. N. Rao, G. George, A. R. Dhakate, K. Salunke, A. Srivastava, and S. A. Rao (2016), Indian summer monsoon rainfall simulation and prediction skill in the CFSv2 coupled model: Impact of atmospheric horizontal resolution, *J. Geophys. Res. Atmos.*, *121*, 2205–2221, doi:10.1002/2015JD024629.
Rauscher, S. A., E. Coppola, C. Piani, and F. Giorgi (2010), Resolution effects on regional climate model simulations of seasonal precipitation over Europe, *Clim. Dyn.*, *35*(4), 685–711.
Roeckner, E., R. Brokopf, M. Esch, M. Giorgetta, S. Hagemann, L. Kornblueh, F. Manzini, U. Schlese, and U. Schulzweida (2006), Sensitivity of simulated climate to horizontal and vertical resolution in the ECHAM5 atmosphere model, *J. Clim.*, *19*, 3771–3791.
Sara, A., R. E. Coppola, C. Piani, and F. Giorgi (2010), Resolution effects on regional climate model simulations of seasonal precipitation over Europe, *Clim. Dyn.*, *35*, 685–711.
Senior, C. A. (1995), The dependence of climate sensitivity on the horizontal resolution of a GCM, *J. Clim.*, *8*(11), 2860–2880.
Seo, K. H., J. Ok, J. H. Son, and D. H. Cha (2013), Assessing future changes in the East Asian summer monsoon using CMIP5 coupled models, *J. Clim.*, *26*(19), 7662–7675.
Shiao, C., and H. H. Juang (2006), Sensitivity study of the climate simulation over East Asia with the CWB regional spectral model, *Terr. Atmos. Oceanic Sci.*, *17*(3), 593–612.
Sperber, K. R., S. Hameed, G. L. Potter, and J. S. Boyle (1994), Simulation of the northern summer monsoon in the ECMWF model: Sensitivity to horizontal resolution, *Mon. Weather Rev.*, *122*(11), 2461–2481.
Sun, X. R., L. X. Chen, and J. He (2002), Index of land-sea thermal difference and its relation to interannual variation of summer circulation and rainfall over East Asian (in Chinese), *Acta Meteorol. Sin.*, *60*, 164–172.
Tang, J., M. Zhao, and B. Su (2007), The effects of model resolution on the simulation of regional climate extreme events, *Acta Meteorol. Sin.*, *21*(2), 129–140.
Tao, S., and L. Chen (1987), A review of recent research on the East Asian summer monsoon in China, in *Monsoon Meteorology*, edited by C.-P. Chang and T. N. Krishnamurti, pp. 60–92, Oxford Univ. Press., New York.
Taylor, K. E. (2001), Summarizing multiple aspects of model performance in a single diagram, *J. Geophys. Res.*, *106*, 7183–7192, doi:10.1029/2000JD900719.
Tibaldi, S., T. N. Palmer, C. Branković, and U. Cubasch (1990), Extended-range predictions with ECMWF models: Influence of horizontal resolution on systematic error and forecast skill, *Q. J. R. Meteorol. Soc.*, *116*(494), 835–866.
Tripathi, O. P., and F. Dominguez (2013), Effects of spatial resolution in the simulation of daily and subdaily precipitation in the southwestern US, *J. Geophys. Res. Atmos.*, *118*, 7591–7605, doi:10.1002/jgrd.50590.
Wang, B., H. Ho, Y. Zhang, and M. Lu (2004), Definition of South China Sea monsoon onset and commencement of the East Asia summer monsoon, *J. Clim.*, *17*, 699–710.
Wehner, M. F., R. L. Smith, G. Bala, and P. Duffy (2010), The effect of horizontal resolution on simulation of very extreme US precipitation events in a global atmosphere model, *Clim. Dyn.*, *34*, 241–247.
Wu, T. (2012), A mass-flux cumulus parameterization scheme for large-scale models: Description and test with observations, *Clim. Dyn.*, *38*, 725–744.
Wu, T., R. Yu, and F. Zhang (2008), A modified dynamic framework for the atmospheric spectral model and its application, *J. Atmos. Sci.*, *65*(7), 2235–2253.
Wu, T., R. Yu, F. Zhang, Z. Wang, M. Dong, L. Wang, X. Jin, D. Chen, and L. Li (2010), The Beijing Climate Center atmospheric general circulation model: Description and its performance for the present-day climate, *Clim. Dyn.*, *34*(1), 123–147.

Wu, T., et al. (2014), An overview of BCC climate system model development and application for climate change studies, *J. Meteorol. Res.*, *1*, 34–56.
Xin, X., T. Wu, and J. Zhang (2012), Introduction of CMIP5 experiments carried out by BCC climate system model (in Chinese), *Adv. Clim. Change Res.*, *8*, 378–382.
Xin, X., T. Wu, J. Li, Z. Wang, W. Li, and F. Wu (2013a), How well does BCC_CSM1.1 reproduce the 20th century climate change over China?, *Atmos. Oceanic Sci. Lett.*, *6*, 21–26.
Xin, X., L. Zhang, J. Zhang, T. Wu, and Y. Fang (2013b), Climate change projections over East Asia with BCC_CSM1.1 climate model under RCP scenarios, *J. Meteorol. Soc. Jpn.*, *91*(4), 413–429.
Yan, H. (1987), Design of a nested fine-mesh model over the complex topography. Part two: Parameterization of the subgrid physical processes (in Chinese), *Plateau Meteorol.*, *6*(suppl.), 64–139.
Yang, B., Y. Zhang, Y. Qian, T. Wu, A. Huang, and Y. Fang (2015), Parametric sensitivity analysis for the Asian summer monsoon precipitation simulation in the Beijing Climate Center AGCM, version 2.1, *J. Clim.*, *28*, 5622–5644.
Zeng, X., M. Zhao, and R. E. Dickinson (1998), Intercomparison of bulk aerodynamic algorithms for the computation of sea surface fluxes using TOGA COARE and TAO data, *J. Clim.*, *11*, 2628–2644.
Zhang, L., T. Wu, and X. Xin (2013), The annual modes of tropical precipitation simulated by Beijing Climate Center climate system model (BCC_CSM) (in Chinese), *Chin. J. Atmos. Sci.*, *37*(5), 994–1012.
Zhou, T., and Z. Li (2002), Simulation of the East Asian summer monsoon using a variable resolution atmospheric GCM, *Clim. Dyn.*, *19*, 167–180.
Zhou, T., Y. Yu, H. Liu, W. Li, X. You, and G. Zhou (2007), Progress in the development and application of climate ocean models and ocean-atmosphere coupled models in China, *Adv. Atmos. Sci.*, *24*, 1109–1120.
Zhou, T., et al. (2009), Why the western Pacific subtropical high has extended westward since the late 1970s?, *J. Clim.*, *22*(8), 2199–2215.
Zhu, C., X. Zhou, P. Zhao, L. Chen, and J. He (2011), Onset of East Asian subtropical summer monsoon and rainy season in China, *Sci. China Earth Sci.*, *54*(12), 1845–1853.